ELSEVIER

Int. J. Therm. Sci. 41 (2002) 73–81

International Journal of Thermal Sciences

Natural convection from an inclined plate embedded in a variable porosity porous medium due to solar radiation

Ali J. Chamkha [a,*], Camille Issa [b], Khalil Khanafer [c]

[a] *Department of Mechanical Engineering, Kuwait University, P.O. Box 5969, Safat, 13060, Kuwait*
[b] *Department of Civil Engineering, Lebanese American University, Byblos, Lebanon*
[c] *Department of Mechanical Engineering, Ohio State University, Columbus, OH 43210-1107, USA*

Received 18 January 2001; accepted 5 March 2001

Abstract

Natural convection boundary-layer flow of an absorbing and electrically-conducting fluid over a semi-infinite, ideally transparent, inclined flat plate embedded in a porous medium with variable porosity due to solar radiation is considered. The governing equations are derived using the usual boundary-layer and Boussinesq approximations and accounting for the presence of an applied magnetic field and an applied incident radiation flux. To account for the heat loss from the plate surface, a convective-type boundary condition is employed there. These equations and boundary conditions are non-dimensionalized and transformed using a non-similarity transformation. The resulting non-linear partial differential equations are then solved numerically subject to the transformed boundary conditions by an implicit iterative finite-difference scheme. Graphical results for the velocity and temperature fields as well as the boundary friction and Nusselt number are presented and discussed for various parametric conditions.

Keywords: Natural convcetion; Porous medium; Solar radiation; Inclined plate; Bedded

Introduction

Thermal buoyancy-induced flow and convective heat transfer in fluid-saturated porous media have been the subject of numerous publications. This interest in the subject stems from various engineering applications in geothermal reservoirs, petroleum industries, transpiration cooling, storage of radioactive nuclear waste materials, separation processes in chemical industries, building thermal insulation, and solar heating systems. Early work on porous media used the Darcy law that neglects important effects such as boundary and inertia effects. Vafai and Tien [1] have reported a pioneering work on the boundary and inertia effects of porous media on convective flow and heat transfer situations. In recent years, enhanced models of porous media have been reported. These models have been applied for simulating more generalized situations such as flow through packed and fluidized beds and liquid metal flow through dendritic structures in alloy casting (Nithiarasu et al. [2]). Some of these models deal with variable porosity effects near the boundary in which the porosity distribution exhibits a peak value there and then decays asymptotically beyond that value. The basis for these models was the early experimental work of Benenati and Brosilow [3] on void fraction distribution in packed beds. Examples of such models are reported and employed by Vafai [4], Vafai et al. [5], Poulikakos and Renken [6], and Nithiarasu et al. [2]. Other models have dealt with thermal dispersion or secondary flow effect in porous media which result from mixing and recirculation of local fluid particles through tortuous paths formed by the spherical particles in packed beds. Examples of these models have been reported by Cheng and Vortmeyer [7] and Amiri and Vafai [8].

Hydromagnetic flows and heat transfer in porous media have been considered extensively in recent years due to their occurrence in several engineering processes such as compact heat exchangers, metallurgy, casting, filtration of liquid metals, cooling of nuclear reactors and fusion control. Ram [9] considered hydromagnetic heat and mass transfer through a porous medium in a rotating fluid. Takhar and Beg [10]

* Correspondence and reprints.
E-mail address: chamkha@kuc01.kuniv.edu.kw (A.J. Chamkha).

1290-0729/02/$ – see front matter
PII: S1290-0729(01)01305-9

Nomenclature

a	absorption or extinction coefficient of fluid	m^{-1}
a_e	effective extinction coefficient of porous medium	m^{-1}
b, c	empirical constants for porosity distribution	
B_o	magnetic induction	tesla
B_f	boundary friction, defined by Eq. (13a)	
c_p	specific heat of fluid	$J{\cdot}kg^{-1}{\cdot}K^{-1}$
C	porous medium inertia coefficient	m^{-1}
d_p	particle diameter	m
Da	porous medium parameter $= a_e d_p$	
F	dimensionless stream function, defined by Eq. (7g)	
g	gravitational acceleration	$m{\cdot}s^{-1}$
G_a	Grashof number based on effective absorption coefficient a_e, defined by Eq. (7f)	
G_x	local Grashof number, defined by Eq. (7e)	
h	heat transfer coefficient to the fluid	$W{\cdot}m^{-2}{\cdot}K^{-1}$
k_e	effective thermal conductivity of porous medium	$W{\cdot}m^{-1}{\cdot}K^{-1}$
K	porous medium permeability	m^2
Nu	Nusselt number, defined by Eq. (13b)	
Pr	effective Prandtl number $= \mu c_p / k_e$	
q''	incident radiation flux	$W{\cdot}m^{-2}$
q''_{rad}	radiation flux distribution, defined by Eq. (6)	$W{\cdot}m^{-2}$
T	dimensional fluid temperature	K
T_{max}	dimensional maximum local fluid temperature	K
T_w	dimensional wall or plate temperature	K
T_∞	ambient temperature	K
u	dimensional tangential or x-component of velocity	$m{\cdot}s^{-1}$
U	heat transfer loss coefficient to surroundings	$W{\cdot}m^{-2}{\cdot}K^{-1}$
v	dimensional normal or y-component of velocity	$m{\cdot}s^{-1}$
x, y	Cartesian coordinates along and normal to the plate, respectively	m

Greek symbols

α	dimensionless heat transfer loss coefficient to surroundings $= U/(k_e a_e)$	
β	volumetric expansion coefficient	K^{-1}
ε	porosity of porous medium	
ε_∞	ambient porosity of porous medium	
η	dimensionless normal distance defined by Eq. (7d)	
μ	dynamic viscosity of fluid $= \rho\nu$	$kg{\cdot}m^{-1}{\cdot}s^{-1}$
ν	kinematic viscosity of fluid	$m^2{\cdot}s^{-1}$
ϕ	plate inclination angle, degrees	
ρ	density of fluid	$kg{\cdot}m^{-3}$
ψ	stream function	$m^2{\cdot}s^{-1}$
σ	electrical conductivity of fluid	$mho{\cdot}m^{-1}$
θ	dimensionless temperature, defined by Eq. (7h)	
θ_{max}	dimensionless maximum fluid temperature	
θ_w	dimensionless wall or plate temperature	
ξ	dimensionless tangential distance, defined by Eq. (7b)	

have reported on the effects of transverse magnetic field on mixed convection flow over a vertical plate embedded in a fluid-saturated porous medium. Chamkha [11] studied hydromagnetic free convection from a vertical plate embedded in a thermally stratified porous medium with Hall effects.

The problem of free convection heat transfer from a vertical flat plate embedded in a fluid-saturated porous medium was studied by Cheng and Minkowycz [12] who obtained similar solutions for situations of power-law function variable wall temperature. Cheng [13] provided an extensive review of early work on free convection in porous media with special regard to applications in geothermal systems. Plumb and Huenefeld [14] have considered non-Darcy natural convection from heated surfaces in saturated porous media. Kim and Vafai [15] have analyzed the problem of natural convection about a vertical plate in porous media. Hong et al. [16] have reported on the effects of non-Darcy and non-uniform porosity on the vertical-plate natural convection in porous media. Neild and Bejan [17] have given an excellent summary of the free convection flow in porous media. Radiation heat transfer in porous media has also been the subject of many researchers. Examples of such studies are the works of Whitaker [18], and Tong and Tien [19]. In the absence of a porous medium, many works have been reported on natural convection from a heated plate such as Kierkus [20], Hassan and Mohamed [21], Elsayed and Fathalah [22] and Fathalah and Elsayed [23]. The latter authors have considered natural convection flow due to solar radiation over a non-absorbing plate with and without heat losses in view of its possible application in solar collectors with direct solar collection using an absorbing fluid. Recently, Chamkha [24] generalized the work of Fathalah and Elsayed [23] include a uniform porous medium. Many authors have reported on the effect of channeling due to the variations in the porosity of the medium close to the boundary and their significant effect on the wall heat transfer (Hong et al. [16] and Poulikakos and Renken [6]). For this reason, it is of special interest in this paper to consider natural convection flow from an inclined, semi-infinite, impermeable flat plate embedded in a variable porosity porous medium due to solar

radiation and in the presence of an externally applied magnetic field. This means that the working fluid is assumed to be absorbing and electrically conducting. The inclined plate is assumed non-reflecting, non-absorbing, ideally transparent and electrically non-conducting in the present work.

Governing equations

Consider steady, laminar, hydromagnetic two-dimensional, radiation-assisted, buoyancy-induced, boundary-layer flow over an impermeable, ideally transparent, semi-infinite, solar radiation-heated, inclined, flat plate embedded in a fluid-saturated porous medium having a variable porosity distribution and in the presence of a magnetic field. The coordinate system is such that **x** measures the distance along the plate and **y** measures the distance normally into the fluid. The schematics of the problem under consideration and the coordinate system are shown in Fig. 1. A magnetic field of constant strength is applied in the negative y direction at all times. Its interaction with the electrically-conducting working fluid produces a resistive force in the negative x direction. This force is called the Lorentz force. The magnetic Reynolds number is assumed to be small so that the induced magnetic field is neglected. In addition, no electric field exists and the Hall effect, the magnetic or Joule heating, and viscous dissipation are all neglected. Far away from the inclined plate, both the surroundings and the Newtonian and absorbing fluid are maintained at a constant temperature T_∞. The porous medium is assumed to be transparent and in thermal equilibrium with the fluid. Both the fluid and the porous medium are opaque for self-emitted thermal radiation. Also, the solar radiation is a collimated beam that is normal to the plate. Due to the heating of the absorbing fluid and the inclined plate by solar radiation, heat is transferred from the plate to the surroundings. As mentioned before, the working fluid is assumed to have heat absorption properties. On the other hand, one may have a non-absorbing fluid. In this situation, the solid porous medium absorbs the incident solar radiation and transmits it to the working fluid by convection. Upon treating the fluid-saturated porous medium as a continuum (see, Vafai and Tien [1]), including the non-Darcian boundary, inertia and variable porosity effects, and assuming that the Boussinesq approximation is valid, the boundary-layer form of the governing equations can be written as (see, Vafai and Tien [1] and Gebhart et al. [25])

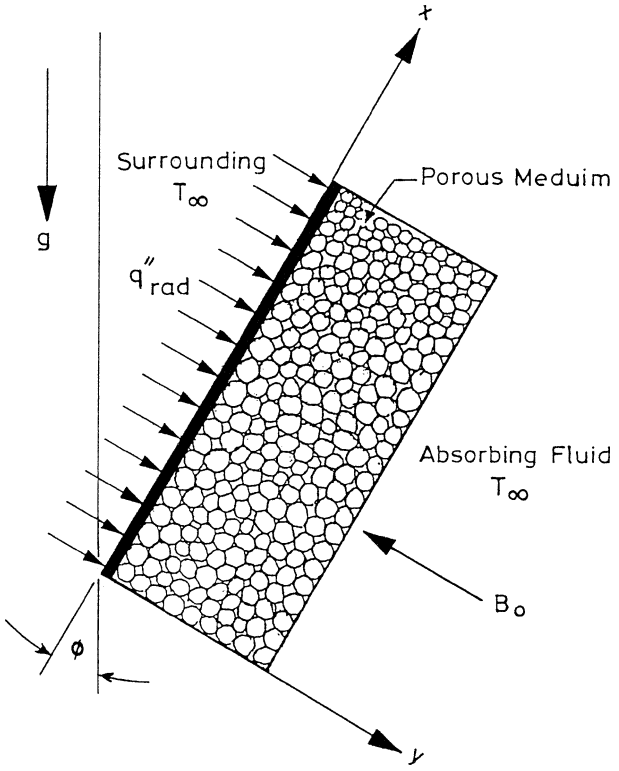

Fig. 1. Flow model and coordinate system.

$$\frac{\partial u}{\partial x}+\frac{\partial v}{\partial y}=0 \tag{1}$$

$$u\frac{\partial u}{\partial x}+v\frac{\partial u}{\partial y}=\nu\frac{\partial^2 u}{\partial y^2}-\frac{\nu}{K(y)}u-C(y)u^2 - \frac{\sigma B_o^2}{\rho}u+g\beta(T-T_\infty)\cos\phi \tag{2}$$

$$u\frac{\partial T}{\partial x}+v\frac{\partial T}{\partial y}=\frac{k_e}{\rho c_p}\frac{\partial^2 T}{\partial y^2}+\frac{1}{\rho c_p}\frac{\partial q''_{rad}}{\partial y} \tag{3}$$

where u, v, and T are the fluid velocity components in the **x** and **y** direction, and the fluid temperature, respectively. ρ, ν, c_p, and σ are the fluid density, kinematic viscosity, specific heat, and electrical conductivity, respectively. $K(y)$, $C(y)$, and k_e are the porous medium permeability, inertia coefficient and effective thermal conductivity, respectively. g, β, ϕ and B_o are the gravitational acceleration, coefficient of volumetric thermal expansion, the inclination angle, and the applied magnetic induction, respectively. q''_{rad} is the applied absorption radiation heat transfer per unit area.

It should be noted in the above equations that all fluid properties are assumed constant except the density in the buoyancy term. In addition, while the effect of porosity variations near the plate are included in the model, the thermal dispersion effects are assumed negligible as done by Poulikakos and Renken [6] and for simplicity. The thermal dispersion effect is minimal when the thermal diffusivity $(k_e/\rho c_p)$ of the porous matrix is of the same order of magnitude as that of the working fluid. This viewpoint of assuming that the effective thermal diffusivity remains constant when the porosity of the porous medium varies with the normal distance is shared by many other investigators such as Vafai [4], Vafai et al. [5] and Tien and Hong [26]. Furthermore, the effect of the motion pressure which arises due to inclination of the plate is expected to be small for the range of angles considered in this work $(0 \leqslant \theta \leqslant 60)$ and, therefore, neglected. This is an acceptable assumption

proven by experiments and is well documented (see, for instance, Gebhart et al. [25]).

The variable porosity model to be supplemented with Eqs. (1) through (3) is the one employed by Poulikakos and Renken [6] in their work on forced convection in porous medium channels and pipes. This model is well established and can be written as

$$K(y) = \frac{d_p^2 \varepsilon^3}{175(1-\varepsilon)^2}$$
$$C(y) = \frac{1.75(1-\varepsilon)}{d_p \varepsilon^3} \tag{4}$$
$$\varepsilon(y) = \varepsilon_\infty \left(1 + b \exp\left(-\frac{cy}{d_p}\right)\right)$$

where d_p is the particle diameter, ε is the porosity of the porous medium, ε_∞ is the porosity near the ambient conditions, and b and c are empirical constants that depend on the ratio of the porous bed to particle diameter (Vafai et al. [5]). As mentioned before, the exponential relation between the porosity and the normal distance from the boundary surface is an approximate representation of the experimental data reported by Benenati and Brosilow [3] for their study on void fraction distribution in packed beds. The values of ε_∞, b, and c employed in the present work are 0.5, 0.98, and 1, respectively. These values were found to give a good approximation to the data reported by Benenati and Brosilow [3] for a particle diameter of 4 mm.

The physics of the problem suggests the following boundary and matching conditions which can be written as

$$u(x,0) = 0 \tag{5a}$$
$$v(x,0) = 0 \tag{5b}$$
$$k_e \frac{\partial T}{\partial y}(x,0) = U\big(T(x,0) - T_\infty\big) \tag{5c}$$
$$u(x,\infty) = 0 \tag{5d}$$
$$T(x,\infty) = T_\infty \tag{5e}$$
$$T(0,y) = T_\infty \tag{5f}$$
$$u(0,y) = 0 \tag{5g}$$

where U is the heat transfer coefficient for the heat lost from the plate to the surroundings. That is, the heat transfer coefficient between the inner surface of the plate and the ambient conditions far from the plate. Eqs. (5a, b) indicate that there is no slip condition and impermeability condition at the surface, respectively. Eq. (5c) indicates that the heat conduction at the plate surface exposed to the fluid is transferred away to the surroundings. Eqs. (5d, e) indicate that far away from the plate the fluid is undisturbed and is at the ambient or surrounding temperature. Eqs. (5f, g) mean that the conditions at the plate's leading edge are such that the fluid is at a uniform temperature and is stagnant.

To complete the problem, information about the radiative absorption function must be supplied. In similar works without a porous medium, Cooper [27] and Fathalah and Elsayed [23] have used Beer's law of radiation absorption and assumed

$$q''_{rad} = q''\big(1 - \exp(-ay)\big) \tag{6}$$

where q'' and a are the incident radiation flux (a constant) and the fluid absorption or extinction coefficient (a constant), respectively. This law was applied to Dorsey's data for the absorption of radiation in water layers of different thicknesses. The estimated value of the extinction coefficient a ranges from 6 m^{-1} to 151.5 m^{-1} for distilled water of thickness 10 cm to 1 mm, respectively. The large variation in the values of a may be attributed to either inaccuracy of Dorsey's measurements as stated by Cooper [27], or to the reflectance and spectral dependence of the absorption coefficient of distilled water, which is not considered by Beer's law as stated by Fathalah and Elsayed [23]. In the absence of experimentally-based proper form of solar energy distribution in a fluid-saturated porous medium, which is a solid-fluid combination, and as a first approximation, Beer's law given by Eq. (6) with an effective absorption coefficient is used in the present work. Therefore, it is assumed that the absorption of solar radiation and its distribution in the porous medium which is made up of transparent solid material such as glass occur in the same manner as they take place in a fluid. This may not be totally true since it is known that normally solid materials respond to radiation differently than a fluid and that the mechanism of travel of radiation rays in solids is different than in a fluid. However, in general, it seems reasonable to assume that the form of Beer's law may be the same for a transparent solid-fluid system but the value of the absorption coefficient will be different. In the presence of a porous solid material the values of a are higher than that of the fluid alone since the system has higher energy capacity. Therefore, the effective extinction coefficient a_e is that of the porous medium. In the present study, an absorption coefficient ranging between 50 m^{-1} and 2000 m^{-1} is assumed for a blackened grey water with transparent glass solid matrix. The average value of radiation flux intensity q'' in Saudi Arabia and Kuwait is about 900 $W \cdot m^{-2}$. The variations in the obtained results as a result of changing the value of a_e are reported in the next section. Thus, the results of this work may be applied to such fluid-saturated transparent porous media that closely exhibit the behaviour of Eq. (6). This clearly highlights the need of extensive experimental effort in this area.

Introducing the stream function ψ and using the transformations employed by Fathalah and Elsayed [23]

$$u = \frac{\partial \psi}{\partial y} \tag{7a}$$
$$v = -\frac{\partial \psi}{\partial x} \tag{7b}$$
$$\xi = \frac{G_x}{G_a^5} \tag{7c}$$
$$\eta = \frac{y G_x}{5x} \tag{7d}$$

$$G_x = 5\left(\frac{g\beta q'' x^4}{5k_e\nu^2}\right)^{1/5} \tag{7e}$$

$$G_a = 5\left(\frac{g\beta q''}{5k_e\nu^2 a_e^4}\right)^{1/5} \tag{7f}$$

$$\psi = \nu G_x F(\xi,\eta) \tag{7g}$$

$$T = T_\infty - \frac{5xq''}{k_e G_x}\theta(\xi,\eta) \tag{7h}$$

where G_x and G_a are the local Grashof number based on the distance along the plate **x** and the Grashof number based on the effective absorption coefficient a_e, respectively in Eqs. (1) through (4) produces

$$F''' + 4FF'' - 3F'^2 - \theta\cos\phi + 4\xi\left(\frac{\partial F}{\partial\xi}F'' - F'\frac{\partial F'}{\partial\xi}\right) - 25\xi^{1/2}\left(\frac{Da^2\varepsilon^3}{175(1-\varepsilon)^2} + M^2\right)F' - 5\xi^{5/4}\frac{(1.75(1-\varepsilon)G_a^5)}{\varepsilon^3 Da}F'^2 = 0 \tag{8}$$

$$\theta'' + Pr\left(4F\theta' - F'\theta\right) - 4\xi Pr\left(F'\frac{\partial\theta}{\partial\xi} - \theta'\frac{\partial F}{\partial\xi}\right) - 5\xi^{1/4}\exp\left(-5\xi^{1/4}\eta\right) = 0 \tag{9}$$

where a prime denotes partial differentiation with respect to η, $Da = a_e d_p$, $M^2 = \sigma B_o^2/(a_e\mu)$, and $Pr = \mu c_p/k_e$ are the porous medium parameter, square of the magnetic parameter or Hartmann number, and the effective Prandtl number, respectively. A representative value for G_a is 1.25 corresponding to water at 5 °C and radiation flux of 900 $W\cdot m^{-2}$.

The transformed form of the variable porosity function becomes

$$\varepsilon(\eta) = \varepsilon_\infty\left(1 + b\exp\left(\frac{-5c\xi^{1/4}}{Da}\eta\right)\right) \tag{10}$$

In addition, the transformed boundary and matching conditions can be shown to be

$$F(\xi,0) = 0 \tag{11a}$$

$$F'(\xi,0) = 0 \tag{11b}$$

$$\theta'(\xi,0) = 5\alpha\xi^{1/4}\theta(\xi,0) \tag{11c}$$

$$F'(\xi,\infty) = 0 \tag{11d}$$

$$\theta(\xi,\infty) = 0 \tag{11e}$$

$$\theta(0,\eta) = 0 \tag{11f}$$

$$F(0,\eta) = 0 \tag{11g}$$

where $\alpha = U/(k_e a_e)$ is the heat transfer loss coefficient. A typical value of α is 0.8 corresponding to an absorbing fluid-matrix system with $a_e = 50\ m^{-1}$ and a surrounding air moving at a speed of 5 $m\cdot s^{-1}$. Larger values of can also be used for higher wind velocities and/or lower values of the effective absorption coefficient a_e.

Of special significance in free convection problems are the local boundary-friction coefficient and the Nusselt number. These physical parameters can be defined in dimensional form as

$$B_f^* = -\mu\frac{\partial^2}{\partial y^2}\psi(x,0) \tag{12a}$$

$$Nu_a = \frac{h}{k_e a_e} \tag{12b}$$

$$h = \frac{q'' - U(T_w - T_\infty)}{T_{max} - T_\infty} \tag{12c}$$

where T_w is the plate or wall temperature, T_{max} is the maximum local temperature, and h is the local heat transfer coefficient. Upon using Eqs. (7a–h), it can be shown that

$$B_f = \frac{B_f^*}{\rho\nu^2 G_x a_e^2} = -\frac{F''(0)}{25\xi^{1/2}} \tag{13a}$$

$$Nu = -\left(\frac{1}{5\xi^{1/4}\theta_{max}} + \alpha\frac{\theta_w}{\theta_{max}}\right) \tag{13b}$$

Numerical procedure

Eqs. (8)–(11) represent the governing equations for the problem under consideration. These equations are nonlinear and, therefore, must be solved numerically by an appropriate numerical scheme. The implicit, iterative, tri-diagonal finite-difference numerical method discussed by Blottner [28] has shown to be successful for the solution of boundary-layer equations. For this reason, it is adopted in the present work.

All first-order derivatives with respect to ξ are replaced by three-point backward-difference formulae. Then, Eq. (8) is converted into a second-order differential equation by making a variable change. Then, all second-order equations in η are discretized using three-point central difference quotients while the first-order equation (obtained from the variable change) is discretized using the trapezoidal rule. With this, the differential equations are converted into a set of algebraic equations at each line of constant ξ. These equations are then solved iteratively (to deal with the nonlinearities of the governing equations) using the Thomas algorithm (see, Blottner [28]). Most changes in the dependent variables are expected to occur in the vicinity of the plate surface where viscous effects are significant. Far away from the wall the fluid adjusts to the ambient conditions and changes in the dependent variables are expected to be small. For this reason, variable step sizes in η are employed in the present work. The initial step size $\Delta\eta_1$ was set to 10^{-3} and the growth factor K^* was set to 1.03 such $\Delta\eta_i = K^*\Delta\eta_{i-1}$. In the majority of the work, $\eta = \infty$ was approximated by $\eta = 10$. In some cases, a larger value was used in order to insure the proper asymptotic approach of both the velocity and temperature to their free-stream values. Constant step sizes in the ξ direction such that $\Delta\xi = 0.01$ are used. These values are arrived at after many numerical experimentations were performed to

assess the accuracy of the numerical results and to insure grid independence. For example, when $\Delta\eta_1$ was set to 0.01, an average error of 5% compared to the case where $\Delta\eta = 10^{-3}$ was obtained. Setting $\Delta\xi = 0.05$ produced an average error of 7% when compared to the case where $\Delta\xi = 0.01$. However, setting $\Delta\eta_1$ and $\Delta\xi$ below 0.001 and 0.01, respectively, produced no significant changes in results. The convergence criterion of the solution required that the relative difference between two successive iterations be 10^{-5}. Many numerical results were obtained throughout the course of this work. A representative set is reported in the next section.

Results and discussion

In this section, the present results are validated with previously published work. In addition, a representative set of results is presented graphically for various parametric conditions and discussed. The parametric values employed in the present work may or may not correspond to a specific application. They are merely chosen to show their effects on the solution.

Fig. 2 shows a comparison for the velocity and temperature profiles at $\xi = 0.1$ in the absence of both the porous medium and magnetic field effects with those reported previously by Fathalah and Elsayed [23]. Good agreement between the results is apparent in this figure. The small differences between the results are due to the fact that Fathalah and Elsayed [23] obtained their results using the local non-similarity method which is less accurate than the current fully-numerical method. For the case of uniform porosity medium, the results are also validated with those reported by Chamkha [24] but not shown here for brevity. These comparisons served as checks on the numerical procedure. Unfortunately, no comparisons with experimental data on this problem were performed because these data do not exist at present.

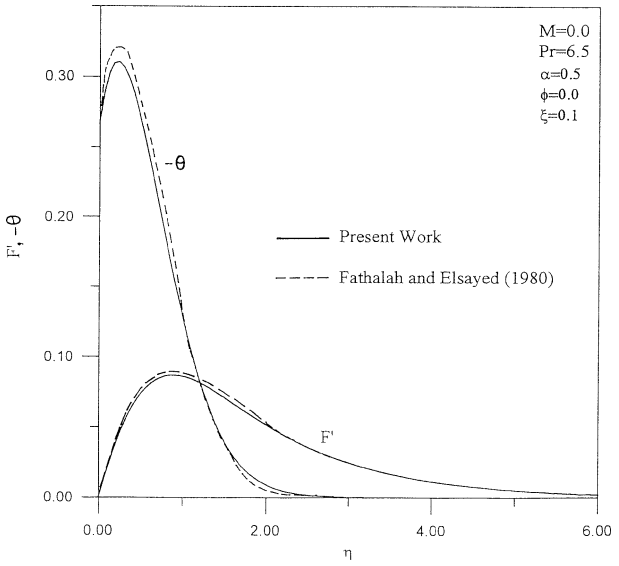

Fig. 2. Comparison of velocity and temperature profiles with Fathalah and Elsayed (1980).

Figs. 3 and 4 illustrate the effects of imposing a magnetic field and increasing its strength on the velocity and temperature profiles at $\xi = 1$, respectively. The reference parametric conditions for which these and all subsequent figures are obtained correspond to water flow along a vertical plate. The imposition of a magnetic field normal to the flow direction produces a resistive force that decelerates the motion of the fluid in the porous medium and along the plate with a resultant increase in the fluid temperature. Fig. 4 also shows that the maximum temperature does not occur at the plate surface but in the region close to it. This is because the incident solar radiation is initially absorbed by the absorbing fluid-matrix system which, in turn, heats up the ideally transparent plate. This operation of passing the absorbing fluid through an absorbing porous medium is believed to enhance solar collection by direct absorption in which heat losses are reduced as a result of lower plate temperatures. In addition, while the hydrodynamic boundary-layer thickness is not affected by the increase in the magnetic field strength, the thermal boundary-layer thickness is significantly increased. These behaviours are depicted in the respective decreases and in-

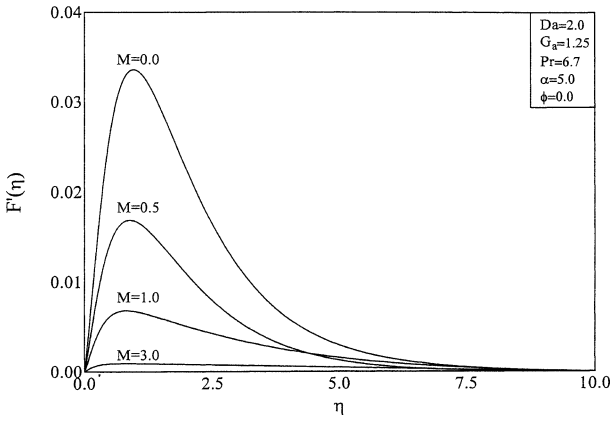

Fig. 3. Effects of M on tangential velocity profiles.

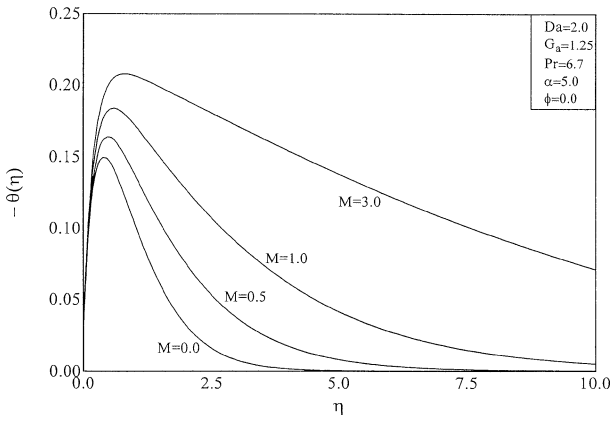

Fig. 4. Effects of M on temperature profiles.

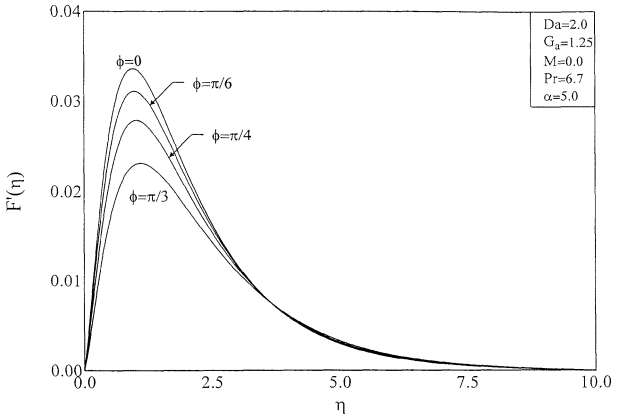

Fig. 5. Effects of ϕ on tangential velocity profiles.

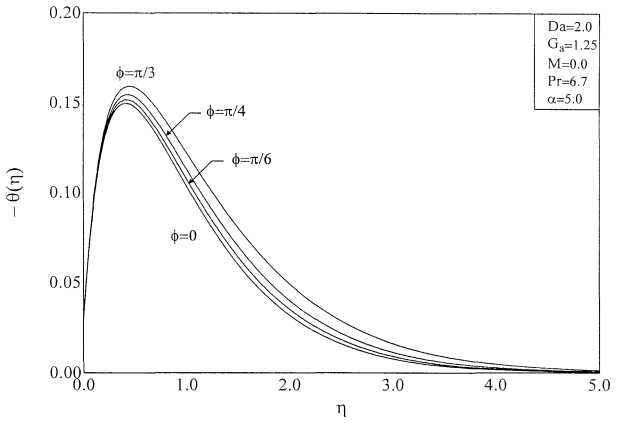

Fig. 6. Effects of ϕ on temperature profiles.

creases in the profiles of F' and θ as the magnetic parameter M is increased.

The influence of the plate inclination angle on the tangential velocity and temperature profiles are displayed in Figs. 5 and 6, respectively. Similar to the effects of the magnetic field, increasing the inclination angle makes it harder for the fluid to flow along the plate and causes it to become warmer. This is due to the reduction in the thermal buoyancy effect ($\beta g(T - T_\infty)\cos\phi$) caused by increases in ϕ. It is obvious that the maximum buoyancy force for the same temperature difference occurs for $\phi = 0$ (vertical plate). This is clearly observed in Figs. 5 and 6.

Figs. 7 and 8 show the influence of the heat transfer loss coefficient to the surrounding on the tangential velocity and temperature profiles, respectively. As the heat loss to the surroundings increases, both the motion and the temperature of the absorbing fluid in the porous medium tend to decrease without significant changes in both the hydrodynamic and thermal boundary layers. These behaviours are clearly evident from the decreases in F' and θ as α increases shown in Figs. 7 and 8. For the case of no heat loss to the surroundings ($\alpha = 0$), Fig. 8 shows that the maximum temperature occurs at the plate surface. This is expected and is consistent with previously published results obtained for non-convective type boundary conditions.

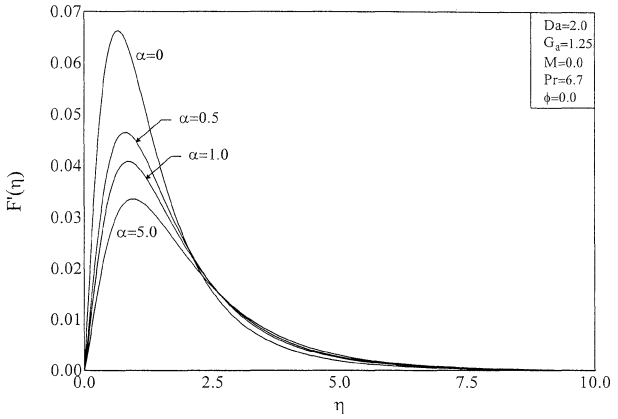

Fig. 7. Effects of α on tangential velocity profiles.

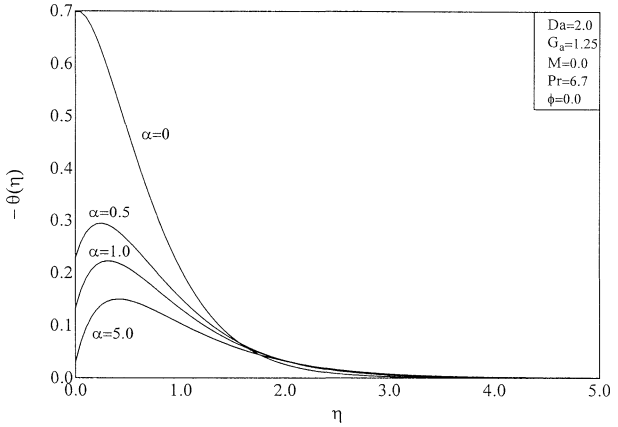

Fig. 8. Effects of α on temperature profiles.

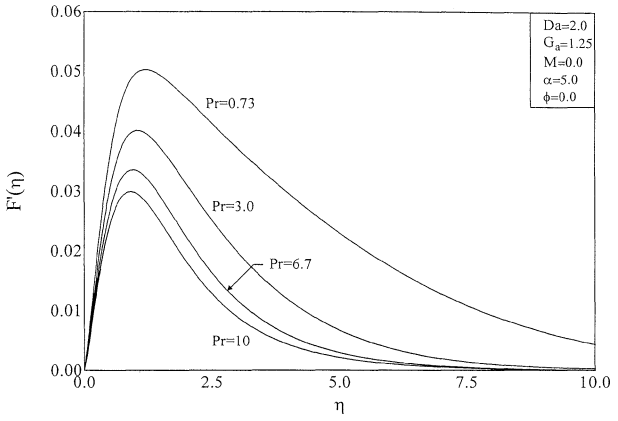

Fig. 9. Effects of *Pr* on tangential velocity profiles.

The effect of varying the effective Prandtl number on the velocity and temperature profiles at $\xi = 1$ is shown in Figs. 9 and 10, respectively. Increases in the values of *Pr* have a tendency to decrease both the fluid temperature and the thermal boundary-layer thickness. This causes a decrease in the thermal buoyancy effect which is causing the fluid flow. Therefore, both the fluid velocity and the hydrodynamic boundary-layer thickness decrease as *Pr* increases. This is clearly displayed in Figs. 9 and 10.

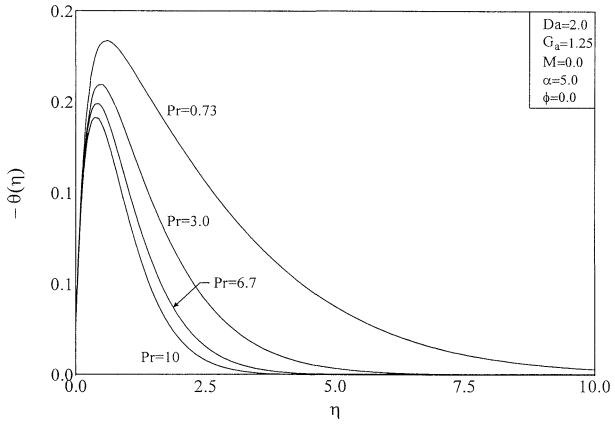

Fig. 10. Effects of *Pr* on temperature profiles.

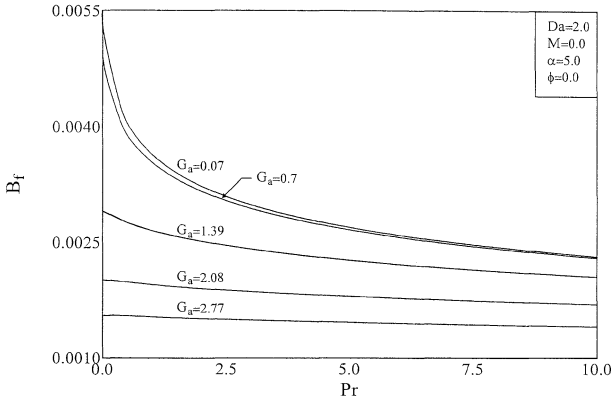

Fig. 11. Effects of *Pr* and G_a on boundary friction coefficient.

Increases in the values of *Da* have a tendency to resist the flow. This, in turn, produces decreases in the tangential velocity and increases in the fluid temperature. In addition, slight increases in the boundary-layer thickness and significant increases in the thermal boundary-layer thickness are observed as a result of increasing *Da*. Also, an observation of Eq. (8) shows that G_a acts as the porous medium inertia effect. Thus, increasing its value represents an increase in the resistance to the flow along the plate. Thus, the fluid velocity decreases while its temperature increases as G_a increases. The degree of reduction in the velocity and increase in the temperature is observed to be larger for $M = 0$ than for $M = 1.0$. These results are not presented here for brevity.

Figs. 11 and 12 depict the variations in the boundary friction coefficient and the Nusselt number that are brought about by simultaneous changes in the values of both the Prandtl number *Pr* and the Grashof number G_a, respectively. Increases in the values of *Pr* have shown in Figs. 9 and 10 to cause reductions in the wall slopes of the tangential velocity profiles and the peak value in the temperature profiles. This indicates that B_f decreases and *Nu* increases with increasing values of *Pr* as is evident from Figs. 11 and 12. On the other hand, increases in the Grashof number G_a result in decreases in both B_f and *Nu*. The decrease in the Nusselt number results from the increases in the maximum

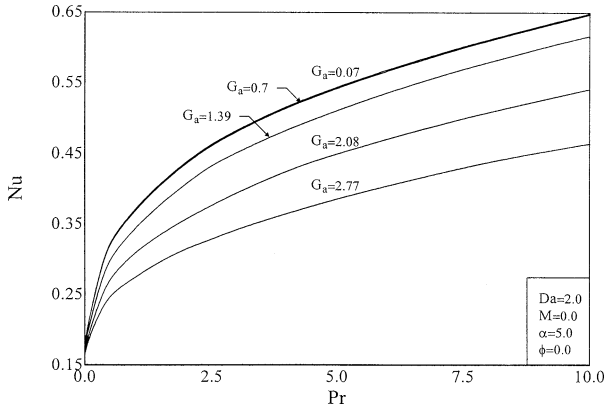

Fig. 12. Effects of *Pr* and G_a on Nusselt number.

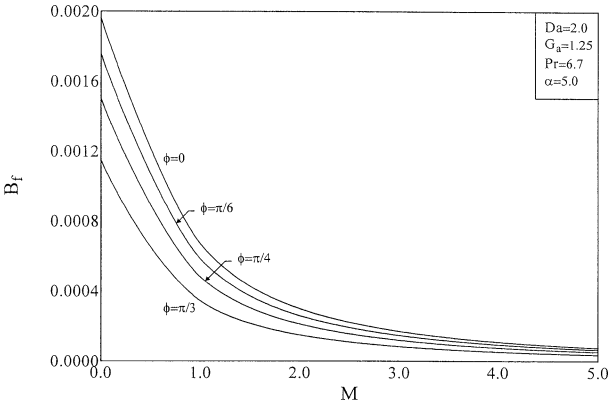

Fig. 13. Effects of *M* and ϕ on boundary friction coefficient.

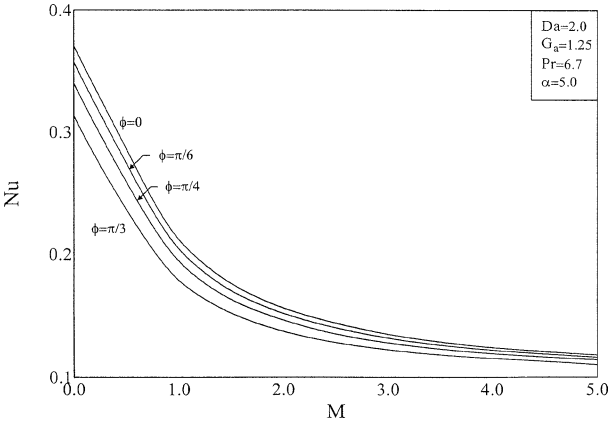

Fig. 14. Effects of *M* and ϕ on Nusselt number.

temperature attained in the flow adjacent to the wall. In addition, Fig. 11 shows that B_f is almost constant for large values of G_a ($G_a = 2.77$) and any value of *Pr*. This is because for $G_a = 2.77$, the resistance mechanism introduced by the inertia effects of the porous medium overcomes all other effects including the thermal buoyancy effect.

Finally, Figs. 13 and 14 display the effects of the inclination angle ϕ and the magnetic parameter *M* on B_f and *Nu*, respectively. Again, by observing Figs. 3–6, one can clearly see that increases in either *M* or ϕ produce reductions

in the wall slope of the velocity profiles and increases in the maximum temperature. This yields simultaneous decreases in the values of B_f and Nu.

Conclusion

Thermal buoyancy-induced, hydromagnetic flow of an absorbing fluid along an inclined, semi-infinite, ideally transparent flat plate embedded in a variable porosity porous medium due to solar radiation is considered. The governing equations are derived using the usual boundary-layer and Boussinesq approximations and accounting for the applied incident radiation flux, magnetic field, and variable porosity effects. A boundary condition to account for heat losses is used at the plate surface. These equations are transformed using a non-similarity transformation and then solved numerically by an implicit, iterative, finite-difference method. Graphical results for the velocity and temperature profiles as well as the boundary friction and Nusselt number are presented and discussed for various parametric conditions. It was found that the boundary friction decreased with increasing values of the effective Prandtl number, heat transfer loss coefficient, inclination angle, Grashof number based on the effective extinction coefficient, heat loss coefficient and the magnetic parameter. However, the Nusselt number was increased as either of the effective Prandtl number or the heat loss coefficient increased and was decreased as either of the magnetic parameter, inclination angle and the Grashof number increased. Comparisons with previously published work were performed and the results were found to be in good agreement. It is hoped that the present work will serve as a stimulus for experimental work which appears to be lacking at present.

References

[1] K. Vafai, C.L. Tien, Boundary and inertia effects on flow and heat transfer in porous media, Internat. J. Heat Mass Transfer 24 (1981) 195–203.

[2] P. Nithiarasu, K.N. Seetharamu, T. Sundararajan, Natural convective heat transfer in a fluid saturated variable porosity medium, Internat. J. Heat Mass Transfer 40 (1997) 3955–3967.

[3] R.F. Benenati, C.B. Brosilow, Void fraction distribution in packed beds, AIChE J. 8 (1962) 359–361.

[4] K. Vafai, Convective flow and heat transfer in variable porosity media, J. Fluid Mechanics 147 (1984) 233–259.

[5] K. Vafai, R.L. Alkire, C.L. Tien, An experimental investigation of heat transfer in variable porosity media, ASME J. Heat Transfer 107 (1985) 642–647.

[6] D. Poulikakos, K. Renken, Forced convection in a channel filled with porous medium, including the effects of flow inertia, variable porosity, and Brinkman friction, ASME J. Heat Transfer 109 (1987) 880–888.

[7] P. Cheng, D. Vortmeyer, Transverse thermal dispersion and wall channeling in a packed bed with forced convective flow, Chem. Engrg. Sci. 43 (1988) 2523–2532.

[8] A. Amiri, K. Vafai, Analysis of dispersion effects and non-thermal equilibrium, non-Darcian, variable porosity incompressible flow through porous media, Internat. J. Heat Mass Transfer 37 (1994) 936–954.

[9] P.C. Ram, Heat and mass transfer on MHD heat generating flow through a porous medium in a rotating fluid, Astrophys. Space Sci. 172 (1989) 273–277.

[10] H.S. Takhar, O.A. Bèg, Effects of transverse magnetic field, Prandtl number and Reynolds number on non-Darcy mixed convective flow of an incompressible viscous fluid past a porous vertical flat plate in a saturated porous medium, Internat. J. Energy Research 21 (1997) 87–100.

[11] A.J. Chamkha, MHD-free convection from a vertical plate embedded in a thermally stratified porous medium with hall effects, Appl. Math. Modelling 21 (1997) 603–609.

[12] P. Cheng, W.J. Minkowycz, Free convection about a vertical flat plate embedded in a porous medium with application to heat transfer from a dike, J. Geophys. Res. 82 (1977) 2040–2044.

[13] P. Cheng, Heat transfer in geothermal systems, Adv. Heat Transfer 4 (1978) 1–105.

[14] O.A. Plumb, J.C. Huenefeld, Non-Darcy natural convection from heated surfaces in saturated porous media, Internat. J. Heat Mass Transfer 24 (1981) 765–768.

[15] S.J. Kim, K. Vafai, Analysis of natural convection about a vertical plate embedded in a porous medium, Internat. J. Heat Mass Transfer 32 (1989) 665–677.

[16] J. Hong, Y. Yamada, C.L. Tien, Effect of non-Darcian and nonuniform porosity on vertical-plate natural convection in porous media, J. Heat Transfer 109 (1987) 356–362.

[17] D.A. Nield, A. Bejan, Convection in Porous Media, Springer, New York, 1992.

[18] S. Whitaker, Radiant energy transport in porous media, Internat. Engrg. Chem. Fund. 19 (1980) 210–218.

[19] T.W. Tong, C.L. Tien, Radiative heat transfer in fibrous insulations — Part 1: Analytical study, ASME J. Heat Transfer 105 (1983) 70–75.

[20] W.T. Kierkus, An analysis of laminar free convection flow and heat transfer about an inclined isothermal flat plates, Internat. J. Heat Mass Transfer 11 (1968) 241–253.

[21] K. Hassan, S. Mohamed, Natural convection from isothermal flat surfaces, Internat. J. Heat Mass Transfer 13 (1970) 1873–1886.

[22] M.M. Elsayed, K.A. Fathalah, Temperature distribution in a direct solar heater, in: 72nd Annual Meeting of AIChE, Nov. 1979, Paper No. P-7d.

[23] K.A. Fathalah, M.M. Elsayed, Natural convection due to solar radiation over a non-absorbing plate with and without heat losses, Internat. J. Heat Fluid Flow 2 (1980) 41–45.

[24] A.J. Chamkha, Solar radiation assisted natural convection in uniform porous medium supported by a vertical flat plate, ASME J. Heat Transfer 119 (1997) 35–43.

[25] B. Gebhart, Y. Jaluria, R.L. Mahajan, B. Sammakia, Buoyancy-Induced Flows and Transport, Hemisphere, New York, 1988, p. 914.

[26] C.L. Tien, J.T. Hong, Natural convection in porous media under non-Darcian and non-uniform permeability conditions, in: Kakac et al. (Eds.), Natural Convection, Hemisphere, Washington, DC, 1985.

[27] P.I. Cooper, Some factors affecting the absorption of solar radiation in solar stills, Solar Energy 13 (1972) 373–381.

[28] F. Blottner, Finite difference methods of solutions of the boundary-layer equations, AIAA J. 8 (1970) 193–205.